Desalination and Water Treatment
www.deswater.com

doi: 10.5004/dwt.2018.21854

102 (2018) 312–325
January

Preparation of a novel activated carbon from jujube stones (*Ziziphus jujuba*) for the removal of basic and acid dyes

Zohra Bahnes[a,*], Noureddine Benderdouche[a], Salima Attouti[a], Benaouda Bestani[a], Laurent Duclaux[b], Laurence Reinert[b]

[a]*Laboratoire de structure, Elaboration et Application des Matériaux Moléculaires (SEA2M), Faculté des Sciences et de la Technologie, Université Abdelahmid Ibn Badis, Mostaganem, Algeria, Tel. +213(0)790540538; Fax:+213(0)45206476; email: zohrabahnes@yahoo.fr (Z. Bahnes), Tel. +213-670310994; email: benderdouchen@yahoo.fr (N. Benderdouche), Tel. +213(0)772618906; email: bestanib@yahoo.fr (B. Bestani), Tel. +213(0)552329407, +213(0)772106195; email: sattouti2010@hotmail.com (S. Attouti)*
[b]*Laboratoire de Chimie Moléculaire et Environnement (LCME), Universite Savoie Mont Blanc, Chambery F-73000, France, Tel./Fax: +33-0-479758805; emails: laurent.duclaux@univ-savoie.fr (L. Duclaux), laurence.reinert@univ-savoie.fr (L. Reinert)*

Received 28 June 2017; Accepted 21 December 2017

ABSTRACT

The present work studies the effect of carbonization temperature, impregnation ratio and activation temperature on the preparation of activated carbon from jujube stones (JB-AC) using potassium hydroxide as an activating agent. Conditions to develop porosity of activated carbon to ameliorate adsorption of Rhodamine B and Orange II dyes were investigated. The effect of various experimental parameters on adsorption such as time, adsorbent dose, pH and temperature was studied to evaluate adsorption capacities of JB-AC. Equilibrium data were analyzed using the well-known Langmuir and Freundlich models. The results indicated that the Langmuir isotherm model was found to best fit adsorption data of both dyes onto the prepared material. Maximum adsorption capacities of Rhodamine B and Orange II onto JB-AC were 207.5 and 498.5 mg/g, respectively. Corresponding results for the commercial Merck activated carbon and jujube stones raw material were 133 and 68.4 mg/g for Rhodamine B and 297.7 and 53.5 mg/g for Orange II. Adsorption kinetics of both dyes followed the pseudo-first-order and pseudo-second-order rate models. Thermodynamic parameters study showed that Rhodamine B and Orange II sorption process on all adsorbents was spontaneous and endothermic. These results show that jujube stones could be valorized into a cost-effective activated carbon that can compete very favorably for the removal of dyes such as Rhodamine B and Orange II from their aqueous solutions.

Keywords: Jujube stones; Activated carbon; Adsorption; Rhodamine B; Orange II

1. Introduction

There are 40,000 dyes and pigments listed in color index, with 7,000 different chemical structures [1]. These dyes contain complex aromatic molecular structure, which make them difficult to biodegrade. Textile industry, food process, cosmetics and pharmaceuticals effluents are colored, representing resented visible pollution. Dye effluents are highly toxic to aquatic life and can cause skin irritation in humans, dermatitis, allergy and cancer [2]. The problems associated with dye pollution could be reduced by various treatment methods including biological, physical and chemical processes such as biodegradation [3], coagulation/flocculation [4], photodegradation [5], sonochemical degradation [6], electrochemical degradation [7] and adsorption [8].

Among these techniques, adsorption is known as one of the most efficient processes to remove dyes from wastewater due to its easy handling, low cost, simple design and

* Corresponding author.

nontoxicity. Adsorption is based on the transfer of pollutants from solution to adsorbent solid phase [9]. Activated carbon is one of the most widely used adsorbents owing to its large surface area and highly developed porosity entailing high capacity for organic matter adsorption.

The high cost of activated carbon has led to develop research in the production of activated carbons from renewable and cheaper precursors such as apricot stones [10], pomegranate peel [11], tea (*Camellia sinensis* L.) [12], sawdust and rice husk [13], doum stone [14], oil palm shell [15] and corncob [16]. Jujube stones are an agro-waste available in large amounts in Algeria in the early fall. This agro-waste is generally disposed of without any use apart from incineration. In the present work, it is used as a precursor for activated carbon preparation as very scarce work has been published about this precursor [17].

Rhodamine B (RhB) and Orange II (OII) are basic and acid dye, respectively, are effluents from textile and paper industries. This study investigates the capacity of an activated carbon prepared from jujube stones by KOH chemical activation for removing RhB and OII. The effect of contact time, adsorbent dose and pH on adsorption was studied.

The Langmuir and Freundlich adsorption isotherms models were fitted to the experimental data and sorption kinetics was evaluated using pseudo-first-order, pseudo-second-order and intraparticle diffusion models. Thermodynamic parameters such as Gibb's free energy ($\Delta G°$), change in enthalpy ($\Delta H°$) and change in entropy ($\Delta S°$) were also evaluated.

2. Materials and methods

2.1. Materials

Jujube stones were collected from the local area of Fornaka in Mostaganem in the west of Algeria. The stones were washed with distilled water and dried at 110°C overnight. Potassium hydroxide (purchased from Sigma-Aldrich-France) of purity 85% was used as chemical activator for the preparation of activated carbon.

RhB was supplied by Merck (Germany) and OII by Fluka (Germany).The chemical structures of the dyes are illustrated in Fig. 1 and the general characteristics of these dyes are given in Table 1.

2.2. Preparation of adsorbent

The dried stones were crushed into small particles (2–5 mm in size) and carbonized in a Nabertherm L3/C6 furnace at temperatures of 300°C, 400°C, 500°C and 600°C at a heating rate of 10°C/min for heating times of 30, 45 and 60 min. The product was characterized for proximate composition, % yield, moisture content (ASTM D2867-70), % ash (ASTM D2866-70), % volatile matters (ISO 562-1981) and % fixed carbon (ASTM D3172).

The char (12.5 g) was impregnated at 25°C with potassium hydroxide (50 mL) at the following (char:KOH) weight ratios 3:1, 2:1, 1:1, 1:2 and 1:3 under continuous overnight stirring. The dried samples were then carbonized at temperatures ranging from 500°C to 800°C for 1–3 h, cooled to room temperature, washed with hydrochloric acid (HCl 0.1 M),

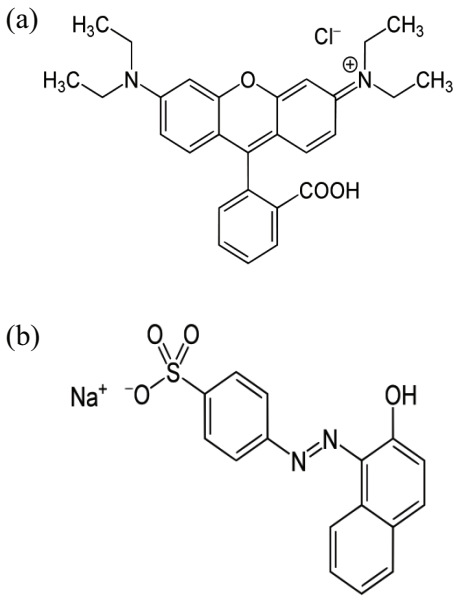

Fig. 1. Chemical structure of (a) Rhodamine B and (b) Orange II.

Table 1
Properties of Rhodamine B and Orange II

	Rhodamine B (RhB)	Orange II (OII)
CI	45,170	15,510
Molecular formula	$C_{28}H_{31}ClN_2O_3$	$C_{16}H_{11}N_2NaO_4S$
Molecular weight (g/mol)	479.02	350.32
Chemical class	Cationic dye	Anionic dye
Molecular volume (Å^3)	–	232 [18]
Maximum wavelength (nm)[a]	555	485

[a]Experimentally obtained values.

rinsed with distilled water and finally in a Soxhlet extractor until the pH of washing effluent reached 7. The activated carbon samples prepared were grinded using a Vierzen Crosshop grinder, sieved through 0.071 mm mesh and stored for further studies [19].

The adsorptive performance of the activated carbon prepared (JB-AC) was compared with that of the jujube stones raw material (JB-R) and commercial Merck activated carbon (MK-AC).

2.3. Adsorbent characterization

2.3.1. Adsorbents porosity and morphology

Jujube stones-based and commercial activated carbons were characterized using the following methods:

- Brunauer-Emmett-Teller (BET) surface area determination using a Micromeritics ASAP 2020 instrument applied in the relative pressure range from 0.01 to 0.05.
- The total pore volume was estimated as the liquid volume of N_2 adsorbed at a relative pressure of 0.995.

- Pore size distributions of the activated carbon samples were determined by using nonlocal density functional theory (NLDFT) models applied on the adsorption isotherms of N_2 at 77 K. Additionally, the distribution of pores smaller than 0.7 nm (narrow micropores or ultramicropores) was evaluated from CO_2 adsorption isotherms at 273 K. For that, infinite slit pores model was assumed for CO_2 adsorption (pores diameter lower than 1.1 nm), while finite slit pores model (2D NLDFT model of finite slit pores having asymmetric ratio of 12) was used for N_2 adsorption simulations [20]. N_2 adsorption data at $P/P_0 < 0.01$ were obtained using incremental fixed doses of ~10 cm^3/g (STP), setting the equilibration interval at 300 s. CO_2 adsorption data were obtained at P/P_0 ranging from 4×10^{-4} to 3.5×10^{-2}, using 45 s equilibration interval because of the quick diffusion of this gas at 273 K [21].
- Iodine number (mg of iodine adsorbed/g of carbon) and methylene blue index (mg of methylene blue adsorbed/g of carbon) determination was performed according to the ASTM D4607-94 and Chemviron Carbon company methods TM-11, respectively [19].

2.3.2. Methylene blue available area (S_{MB})

Methylene blue adsorption on activated carbons is used for specific surface area determination, especially mesoporosity. A mass of 0.1 g of studied material is mixed with 25 mL of methylene blue solution at different concentrations; the mixture is stirred for 2 h then filtered and analyzed. The Langmuir isotherm can be used to calculate the area available for Methylene blue by the following Eq. (1):

$$S_{MB} = \frac{b \cdot N \cdot S}{M} \tag{1}$$

where S_{MB} is the specific surface area (m^2/g), b is the maximum adsorption capacity (mg/g; it can be determined from the Langmuir isotherm), N is Avogadro's number (6.023×10^{23}), S is the area occupied by a methylene blue molecule (119 $Å^2$) and M is the molecular weight methylene blue (319.86 g/mol).

2.3.3. Zero point of charge determination (pH_{zpc})

The zero point charge of the carbon (pH_{zpc}) is defined as the pH of the suspension at which positive or negative charge was absent on the surface of activated carbon. It was determined as follows: a mass of 0.15 mg of each adsorbent was introduced into an aqueous NaCl solution (50 mL 0.01 mol/L) and the pH was adjusted to successive initial values between 2 and 12. The suspensions were stirred during 48 h and the final pH was measured and plotted as a function of the initial pH. The pH_{ZPC} is determined at the value for which $pH_{final} = pH_{initial}$.

2.3.4. Functional groups analysis (FTIR)

IR spectroscopic analysis employing the KBr pellet technique at room temperature using an IR Prestige-21 SHIMADZU spectrophotometer in the scanning range of 4,000–400 cm^{-1} was performed on the adsorbents to identify the principal chemical functional groups present on adsorbents surface.

2.4. Adsorption studies

Organic dye adsorption onto activated carbons has been studied by several authors [22,23]. Batch adsorption experiments of RhB and OII dyes on the different adsorbents prepared (JB-AC, JB-R and MA-AC) were carried out by studying the effect of operating parameters such as contact time (30–360 min), adsorbent dose (2–20 g/L) and pH (2–12) which was adjusted using 0.1 N NaOH or 0.1 N HCl.

In a series of 250 mL capped Erlenmeyer flasks at a room temperature 25°C ± 1°C, 25 mL of a dye solution of known initial concentration was mixed with a known amount of adsorbent. The suspension was magnetically stirred at 600 rpm until equilibrium was reached, then centrifuged at 4,000 rpm for 15 min and the residual dye concentration measured by spectrophotometry at maximum wavelength shown in Table 1. The amount of dye adsorbed per gram of adsorbent (q_e) was calculated by the following relationship (Eq. (2)):

$$q_e = \frac{\left(C_0 - C_{eq}\right)}{1{,}000\ \mathrm{m}} V \tag{2}$$

where C_0 and C_{eq} are the initial and equilibrium dye concentrations (mg/L), V is the volume of the liquid phase (mL) and m is the mass of adsorbent used (g).

3. Results and discussions

3.1. Jujube stone activated carbon preparation

3.1.1. Carbonization

Carbonization was carried out in the temperature range 300°C–600°C in a muffle furnace for 30–60 min. Yield (Y), moisture (M), volatile matters (VM), ash and fixed carbon (FC) percentage values are presented in Table 2. It can be seen that yield and volatile matters of jujube stone char decreased with carbonization temperature due to dehydration and thermal degradation of cellulose. A large yield decrease (60.13 down to 27.25) occurred when temperature was increased from 300°C to 400°C but for higher temperatures a slow yield was observed in agreement with other works [24].

Fixed carbon indicates char carbon and increases with carbonization temperature and heating time. The ash content is a measure of the nonvolatile matter and noncombustible component of the char [25]. The jujube stones char prepared at 500°C during 60 min containing 25.832% of volatile matters and 65.394% of fixed carbon is suitable for the next activation step as the percentage volatile matter is convenient in the range 20%–25% [26].

3.1.2. Effect of KOH impregnation ratio

Activated carbon samples were prepared by potassium hydroxide as a chemical activating agent at the following char:KOH weight ratios 3:1, 2:1, 1:1, 1:2 and 1:3. The results of both iodine number and methylene blue index are

summarized in Table 3. Iodine number increased regularly attaining a maximum of 1,358 mg/g at the weight ratio 1:2 while the methylene blue index reached 299.35 mg/g at the ratio 1:3. The iodine number decrease can be explained by a reduction in microporosity. The biological constitution of the material used disaggregates and becomes disordered at a strong base concentration, which favors pore destruction instead of their creation.

3.1.3. Effect of activation temperature and time

Further tests were carried out by varying the activation temperature from 500°C to 800°C at various carbonization times (1, 2 and 3 h). From Table 3, it can be seen that burn-off (%), iodine number and methylene blue index increased with temperature between 500°C and 700°C for the range of carbonization time investigated. At a temperature of 800°C, burn-off increased rapidly up to a maximum value of 84.48% with a reduction of both indices. Such a high burn-off which would not contribute to the creation of micropores could be attributed to a deep activation process that involves burning of the wall between neighboring pores [27]. The maximum values of iodine number and methylene blue index of 1,358 and 299 mg/g were obtained for the impregnation ratio 2:1 (KOH:char) and 700°C activation temperature for a 3 h carbonization time.

3.2. Characterization of adsorbents

The N_2 and CO_2 adsorption–desorption isotherms of the JB-AC and MK-AC are shown in Fig. 2. The JB-AC nitrogen adsorption isotherm corresponds to type I isotherms according to IUPAC classification [28,29]. It is clear that adsorption becomes saturated after very low relative pressure regions (P/P_0 > 0.2) indicating that JB-AC is a microporous material in accordance with the obtained high iodine number

Table 2
Proximate analysis of jujube stones char at different temperatures and times

Temperature (°C)	Time (min)	*Y* (%)	*M* (wt%)	Ash (wt%)	VM (wt%)	FC (wt%)
300	30	60.131	5.655	1.663	60.185	32.495
	45	54.193	4.51	0.892	54.743	39.926
	60	49.176	3.532	1.641	49.33	45.492
400	30	29.718	8.986	1.751	34.150	55.111
	45	28.443	4.198	2.184	32.219	61.398
	60	27.256	6.323	1.965	30.735	60.976
500	30	27.393	8.087	2.431	28.507	60.974
	45	23.562	5.656	2.216	28.370	63.757
	60	23.034	6.487	2.286	25.832	65.394
600	30	21.739	6.141	1.37	12.201	80.285
	45	23.171	6.421	2.928	11.889	78.761
	60	20.91	6.143	2.23	16.64	74.986

Table 3
Iodine number and methylene blue index values as a function of KOH concentration, and activation temperature at various carbonization times

	KOH concentration (char:KOH ratio)				
	3:1	2:1	1:1	1:2	1:3
Iodine number (mg/g)	853.22	941.44	1,038.66	1,358.05	1,188.24
Methylene blue index (mg/g)	211.36	227.95	242.73	299.02	299.35

	Temperature (°C) at various carbonization times (h)[a]											
	500			600			700			800		
Carbonization time (h)	1	2	3	1	2	3	1	2	3	1	2	3
Iodine number (mg/g)	375.43	389.46	392.27	403.58	535.25	600.89	872.26	891.63	1,358.05	1,296.01	1,322.76	1,302.59
Methylene blue index (mg/g)	71.82	55.45	78.64	76.36	85.91	61.36	228.75	285.89	299.02	276.73	219.77	217.5
Burn-off (%)	43.63	45.04	46.48	49.28	50.00	50.88	52.64	55.52	58.64	75.52	82.00	84.48

[a]Impregnation char:KOH ratio 1:2.

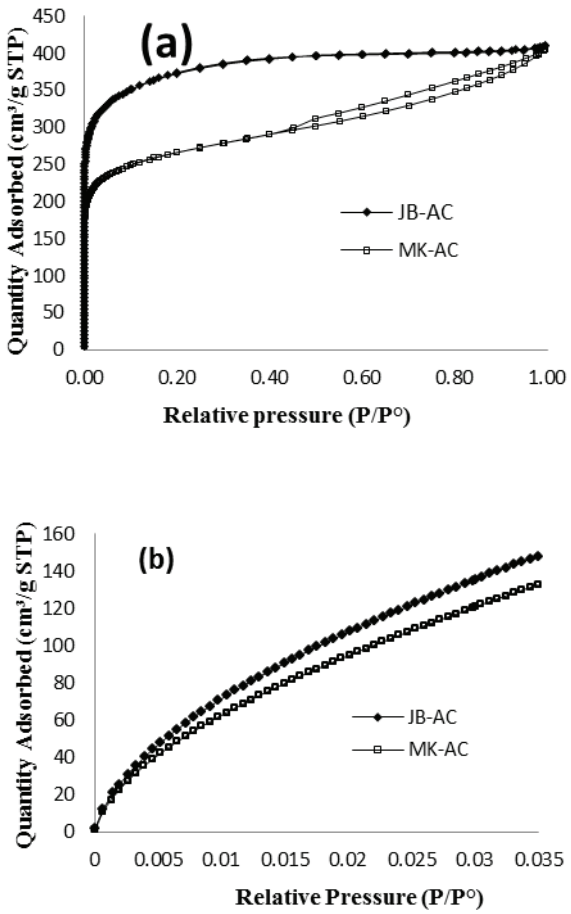

Fig. 2. Adsorption/desorption isotherms of jujube stone activated carbon (JB-AC) and Merck activated carbon (MK-AC). (a) N_2/77 K and (b) CO_2/273 K.

(1,358 mg/g). On the other hand, MK-AC displays type IV isotherm behavior [30]. The narrow hysteresis loops is commonly associated with the presence of mesoporosity at high relative pressures of N_2 ($0.4 < P/P_0 < 1$). The pore size distributions of JB-AC and MK-AC shown in Fig. 3 were calculated using the density functional theory (DFT) model for N_2 adsorption at 77 K and CO_2 at 273 K. The pore size distribution of JB-AC illustrates a large proportion of pores of diameter <3 nm, with lower than 2.0 nm diameter pores accounting for a majority percentage. CO_2 adsorption isotherms at 273 K were recorded for calculating the ultramicropore volume ($V_{ultramicro}$) because the smaller kinetic diameter of the CO_2 molecule (CO_2: 3.3 Å; N_2: 3.6 Å) and the adsorption of CO_2 at relatively high temperatures is a suitable approach to probe such ultramicropores [31]. JB-AC showed better performance for CO_2 adsorption than MK-AC with $V_{ultramicro}$ = 0.394 cm³/g. Table 4 summarizes the values of the specific surface area, total pore volume, total micropore (ultramicropore and supermicropore) volume and mesopore volume of the ACs investigated. The obtained BET surface area and total pore volume for JB-AC were 1,400 m²/g and 0.607 cm³/g while MK-AC corresponding values were 1,017 m²/g and 0.626 cm³/g, respectively. Micropores roughly represent 91% of the total pore volume for JB-AC and 41% for MK-AC. JB-AC exhibited a pore volume primarily in the

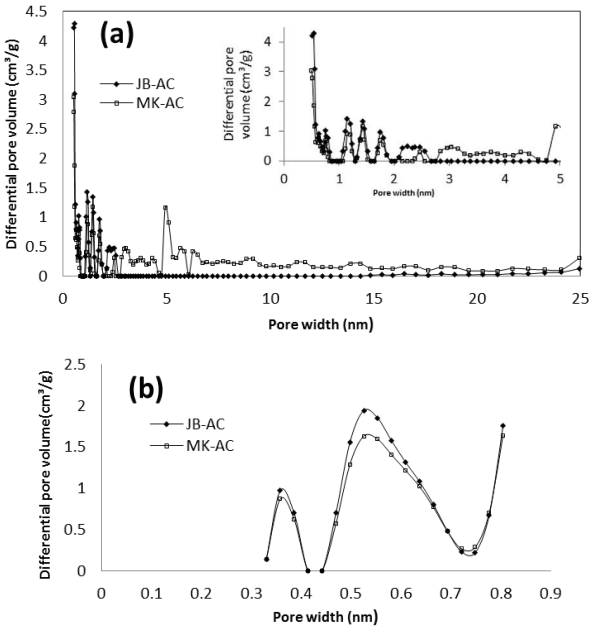

Fig. 3. Pore size distributions of JB-AC and MK-AC calculated using the DFT model. (a) N_2 adsorption at 77 K and (b) CO_2 adsorption at 273 K.

Table 4
Physicochemical characteristics of the adsorbents studied

Property	Adsorbent		
	JB-AC	MK-AC	JB-R
S_{BET} (m²/g)	1,400	1,017	–
S_{MB} (m²/g)	1,120	800	51
$V_{poreux\ total}$ [a] (cm³/g)	0.607	0.626	–
V_{meso} [a] (cm³/g)	0.051	0.242	–
$V_{micro\ total}$ [a] (cm³/g)	0.556	0.383	–
$V_{supermicro}$ [b] (cm³/g)	0.165	0.105	–
$V_{ultramicro}$ [c] (cm³/g)	0.394	0.314	–
Iodine number (mg/g)	1,358	830	200
Methylene blue index (mg/g)	299	173	25
pH_{zpc}	7	6.5	5.2
Ash content (%)	1.69	8.2	1.3

[a]Calculated from N_2/77 K adsorption isotherms.
[b]Calculated from N_2/77 K adsorption isotherms (0.8 < pore diameter < 2 nm).
[c]Calculated from CO_2 adsorption isotherms at 273 K (0.3 < pore diameter < 0.8 nm).

micropore range with a small value of mesopore volume (V_{meso} = 0.051 cm³/g) as well as a high methylene blue index (MB_{index} = 299 mg/g) because the MB molecules are mainly adsorbed in the micropores, with a minimum pore size of 1.33 nm as mentioned in the study of Graham [32].

The pH_{zpc} value for JB-R, MK-AC and JB-AC was found to be 5.2, 6.5 and 7, respectively.

Fig. 4 displays the FTIR spectra obtained for the raw material (JB-R) and the prepared activated carbon (JB-AC). The IR spectra of the MK-AC sample were reported elsewhere [19].

The most important functional groups for all adsorbents are summarized in Table 5. The FTIR data of raw material indicates the presence of bands at 3,420 cm^{-1} and in the ranges 1,630–1,605, 1,384–1,348, 1,240–1,114 and 760–615 cm^{-1} which may be ascribed to the vibration of hydrogen group alcohols (–OH), carbonyl groups (C=O) for ketones and carboxylic acid, carboxylate ion (COO^-), C–O bonds in the alcohols or esters and the aromatic rings or C–H bonds, respectively. The spectrum for JB-AC shows the new band observed at 2,925–2,850 cm^{-1} which can account for C–H stretching vibrations of CH_2 groups [8]. The broad band at 3,700 cm^{-1} may be assigned to –OH stretching vibration. The peaks at 1,740–1,620, 1,460 and 1,118 cm^{-1} can be attributed to C=O, COO– and C–O stretching vibrations, respectively.

3.3. Adsorption parameters

3.3.1. Effect of contact time on adsorption

In order to determine the contact time necessary for each adsorption system to attain equilibrium, experiments were conducted in batch mode by mixing 25 mL of dye solution of a known concentration with 0.1 g of each adsorbent (JB-AC, MK-AC and JB-R) separately. The mixtures were agitated for contact times ranging from 30 to 360 min. After filtration, the equilibrium concentrations of RhB and OII were determined by spectrophotometry. It is clear from Fig. 5 that contact times of 40 and 60 min were sufficient for the removal of OII and RhB with JB-R, while in the case of JB-AC and MK-AC, adsorption increased from 60 to 120 min and thereafter became almost constant. The contact time for the removal of

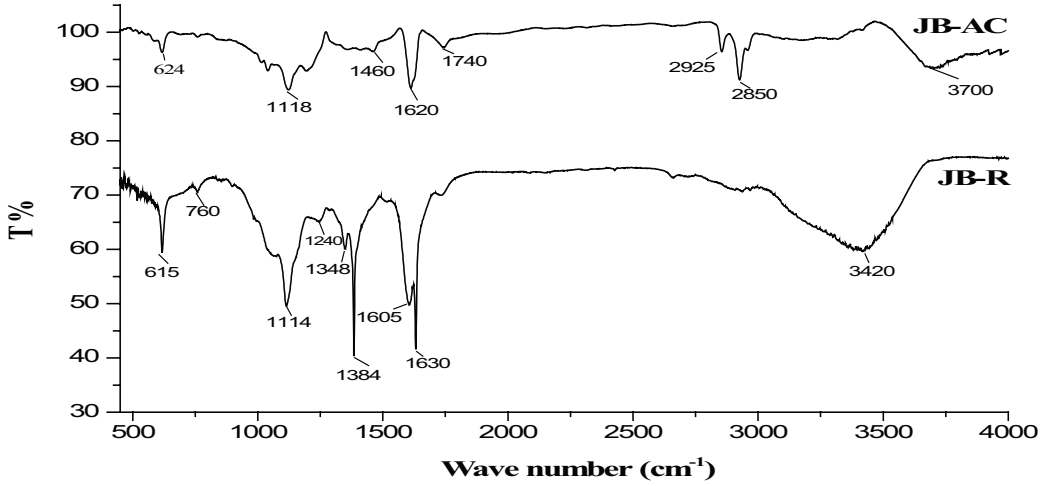

Fig. 4. FTIR spectrum of the JB-AC and JB-R adsorbents.

Table 5
FTIR spectra band assignments for JB-AC, MK-AC and JB-R

Adsorbent	Range (cm^{-1})	Assignment
JB-AC	3,700	Stretching vibration of O–H groups
	2,925–2,850	C–H stretching vibrations of CH_2
	1,740–1,620	C=O stretching band from the carboxyl or ester groups
	1,460	Symmetric stretching vibration, carboxylates COO^-
	1,118	Stretching vibration C–O (of alcohols), =C–O–C= and C–C alkenes
MK-AC[a]	3,619.8–3,092.8	Stretching vibration of O–H groups
	3,021	O–H and $–NH_3^+$ groups
	2,147.3	–C=CN, –N=C–H and –N=C=S group
	1,517.9	Related to N–H bending and C–N stretching
	1,106.6–1,000	C–O bond, characteristics peak for P band
	809–841.7	Alkenes, =C–H bond, stretching vibration N=O
JB-R	3,420	Vibration of hydrogen group alcohols (–OH)
	1,630–1,605	Carbonyl group (C=O) for ketones and carboxylic acid
	1,384–1,348	Stretching vibration of carboxylate ion (COO^-)
	1,240–1,114	Vibrations of the C–O bonds in the alcohols or esters
	760–615	C–H bonds or aromatic rings

[a]From Douara et al. [19].

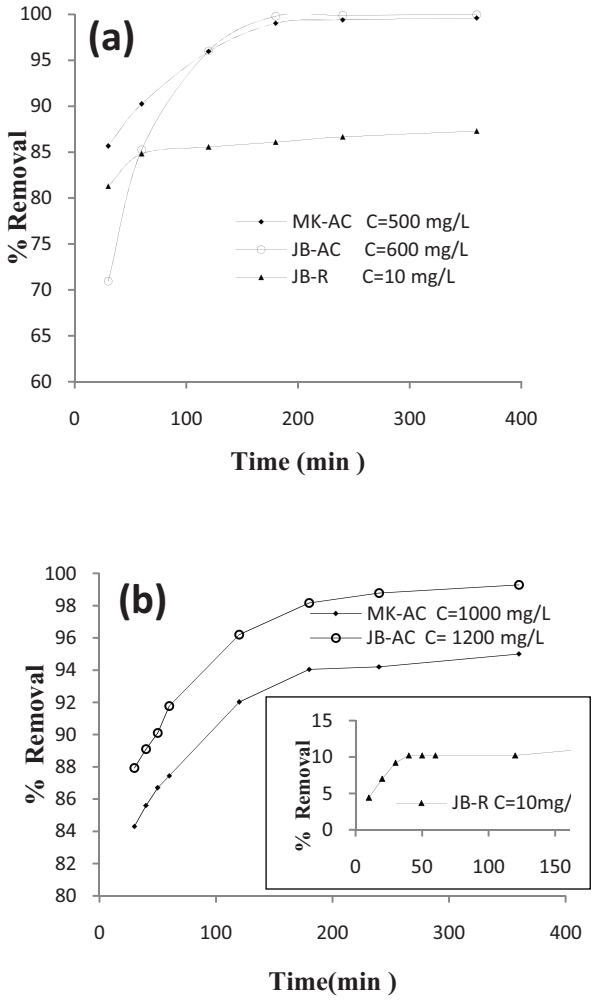

Fig. 5. Effect of contact time on adsorption of (a) RhB and (b) OII by all three considered adsorbents.

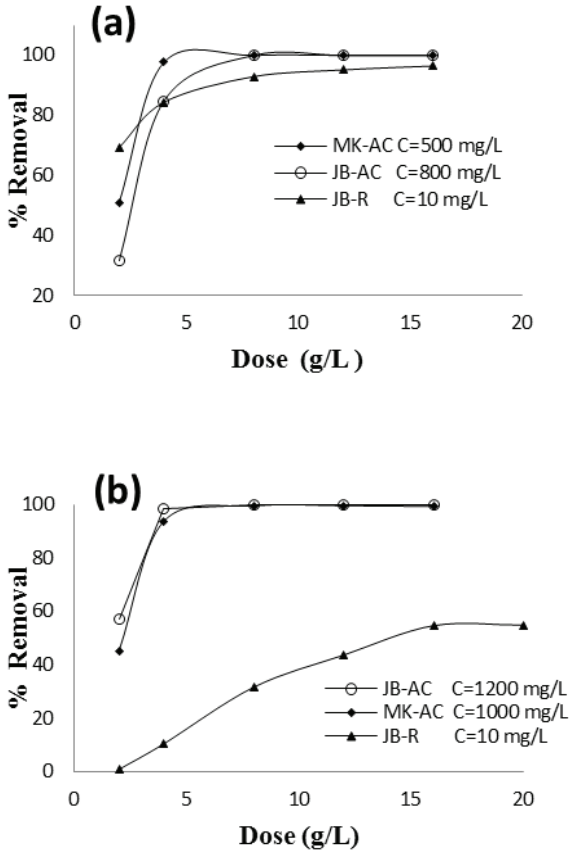

Fig. 6. Effect of adsorbent dose on adsorption of (a) RhB and (b) OII by the adsorbents investigated.

both dyes was chosen as 180 min. These observations show that the rapid adsorption at the beginning may be due to the large number of vacant sites available on the adsorbent surface but as time proceeds, the emergence of the plateau indicates the attainment of the equilibrium process. Similar results were reported by Kooh et al. [33].

3.3.2. Effect of adsorbent dose

The effect of adsorbent dose on dye removal was investigated by changing the quantity of adsorbent (JB-AC, MK-AC or JB-R) within the range 2–20 g/L while maintaining all other parameters constant. As shown in Fig. 6, the maximum uptake of RhB and OII was obtained at an adsorbent dose of 8 g/L onto JB-AC and MK-AC, where most of the dyes (>99%) was removed but for JB-R, the corresponding adsorbent dose was 8 g/L for RhB and 16 g/L for OII. These results show that the percentage removal of both colorants increased with adsorbent dose, which can be attributed to increased surface area and the availability of more adsorption sites [34].

3.3.3. Effect of pH

pH is an important factor in determining the potential for adsorption of cationic and anionic dyes as it may affect adsorbent surface charge and adsorbate ionization. To assess the influence of pH on dye adsorption, adsorption experiments of RhB and OII for various concentrations were carried out at 25°C and solution pH varied from 2 to 12 by adding either 0.1 N NaOH or 0.1 N HCl.

The maximum uptake of the RhB was at pH = 2 for both activated carbons (JB-AC and MK-AC) and pH = 4 onto JB-R. Removal percentage decreased for higher pH values for each adsorbent as shown in Fig. 7(a). This can be explained by the fact that at pH values lower than 4.5, RhB ions are capable of entering into the pore structure while for pH values higher than 4.5, the RhB zwitterions may aggregate to form a bigger molecular form (dimer) and become unable to enter into the adsorbent pore structure. In the water, the greater aggregation of the zwitterionic form is due to the attractive electrostatic interaction between the carboxyl and xanthane groups of the monomer [35].

As shown in Fig. 7(b), the percentage dye removal decreased only from 99.93% to 82.44% and from 85.21% to 75.28% onto JB-AC and MK-AC, respectively, for the same concentration (C = 2,800 mg/L). This result shows that JB-AC is a potentially performant adsorbent for dyes of this kind.

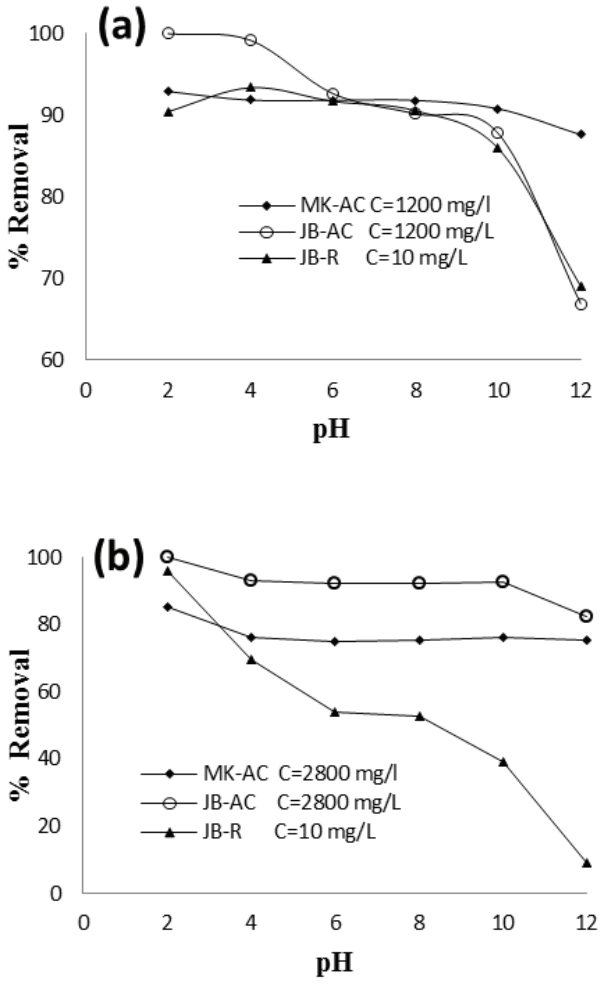

Fig. 7. Effect of pH on adsorption of (a) RhB and (b) OII by all three considered adsorbents.

The maximum percentage dye removal for OII was recorded at pH = 2 for all adsorbents. For a pH less than pH_{zpc}, the charge at the adsorbent surface is positive which has the effect of attracting the negative portion of the anionic dyes [36,37]. pH_{pzc} values for the three adsorbents JB-R, MK-AC and JB-AC were 5.2, 6.5 and 7, respectively.

3.4. Adsorption isotherms

To optimize the design of an adsorption system for the adsorption of adsorbates, it is important to establish the most appropriate correlation for the equilibrium curves. Various isotherm equations such as Langmuir and Freundlich adsorption isotherms were used. Langmuir isotherm assumes the energy of adsorption on the surface of the sites within the adsorbent is uniform and no interaction between the adsorbed molecules, even on adjacent sites [38]. The nonlinear form of the Langmuir (Eq. (3)) adsorption isotherm is given as:

$$q_e = b\frac{K_L C_e}{1+K_L C_e} \tag{3}$$

which can be linearized to:

$$\frac{C_e}{q_e} = \frac{1}{K_L b} + \frac{1}{b}C_e \tag{4}$$

where q_e is amount of dye adsorbed per unit weight of adsorbent (mg/g) and C_e is the equilibrium concentration of dye (mg/L). The nonlinear plot of q_e vs. C_e as well as the linear plot of C_e/q_e vs. C_e allows both the maximum adsorption capacity corresponding to complete monolayer coverage b (mg/g) and the Langmuir constant related to adsorption energy K_L (L/mg) to be obtained.

The essential characteristics of the Langmuir isotherm can be expressed in terms of a dimensionless factor called equilibrium parameter (R_L, also called separation factor) which is defined by the following Eq. (5):

$$R_L = \frac{1}{1+K_L C_0} \tag{5}$$

where C_0 (mg/L) is the initial adsorbate concentration and K_L (L/mg) is the Langmuir constant related to the energy of adsorption. The value of R_L indicates the shape of the isotherm to be either unfavorable ($R_L > 1$), linear ($R_L = 1$), favorable ($0 < R_L < 1$) or irreversible ($R_L = 0$) [39].

The second model used here is the Freundlich model [40]. The Freundlich model has been widely used to describe adsorption data on heterogeneous adsorbent surface. In this case, it is assumed that the stronger binding sites are occupied first and that the binding strength decreases with an increasing degree of site occupation. The nonlinear form of the Freundlich isotherm is represented by the following equation:

$$q_e = K_F C_e^{1/n} \tag{6}$$

whereas the linear form is given by:

$$\log q_e = \log K_F + \frac{1}{n}\log C_e \tag{7}$$

where K_F and n are the physical constants of the Freundlich isotherm can be obtained by plotting q_e vs. C_e or $\log q_e$ vs. $\log C_e$. K_F is the constant indicative of the relative adsorption capacity of the adsorbent $1/n$ of the adsorption intensity and of the type of isotherm, that is, irreversible ($1/n = 0$), favorable ($0 < 1/n < 1$) and unfavorable ($1/n > 1$).

As can be seen from Fig. 8, the equilibrium amount adsorbed increased with dye concentration and became almost steady value for equilibrium concentrations exceeding 400 mg/L. Figs. 9 and 10 show the linearized forms of both models. The adsorption of both dyes obeys the Langmuir isotherm model with determination coefficients R^2 higher than 0.99 for all the adsorbents studied, which confirms the applicability of the Langmuir model for the considered adsorbents, except the adsorption of the RhB onto JB-R with $R^2 = 0.96$ where adsorption data can be better described by the Freundlich equation with $R^2 > 0.99$.

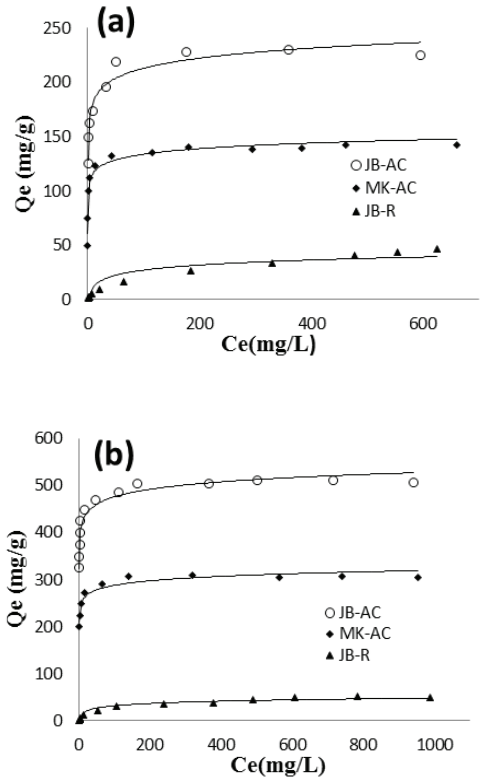

Fig. 8. Adsorption isotherms for (a) RhB and (b) OII onto the adsorbents studied.

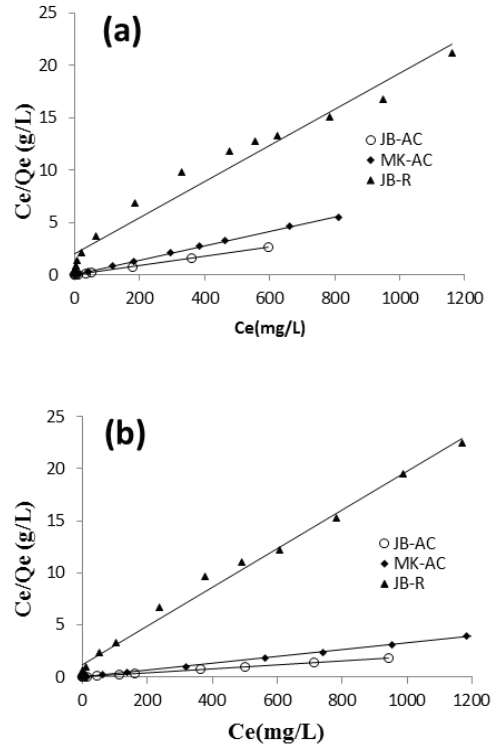

Fig. 9. Linearized Langmuir adsorption isotherms for (a) RhB and (b) OII for the adsorbents studied.

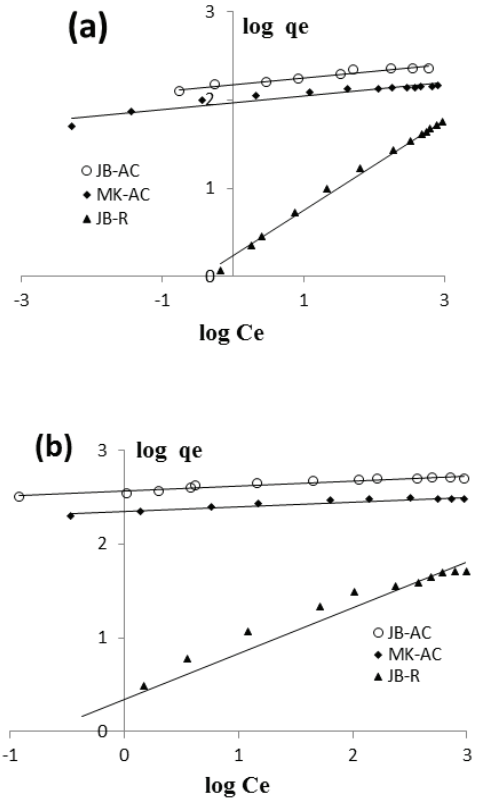

Fig. 10. Linearized Freundlich adsorption isotherms for (a) RhB and (b) OII for the adsorbents studied.

Table 6 summarizes the values of the linearized and nonlinear isotherms calculated parameters. The nonlinear calculated values give slightly lower values than the linear ones but both methods can be applied. The results obtained of the R_L values were in the range between 0 and 1, which shows that adsorption of RhB and OII on the adsorbents was favorable. The high values of K_F indicated that JB-AC and MK-AC had a higher adsorption capacity and affinity for RhB and OII. The values of the exponent $1/n$ were in the range of 0 and 1, indicating favorable adsorption of both dyes.

The higher adsorption capacities of 207.54 and 498.5 mg/g for RhB and OII onto JB-AC as determined from nonlinear Langmuir model fitting in comparison with MK-AC show porosity and specific surface area were significantly enhanced by potassium hydroxide activation. JB-AC also competes favorably with many other adsorbents as shown in Table 7.

3.5. Adsorption kinetics

To control the residence time of adsorbate uptake at the solid–solution interface, three kinetic models, namely, the pseudo-first-order, pseudo-second-order and intraparticle diffusion models [47,48] were investigated and can be expressed in their nonlinear and linear forms respectively as:

- Pseudo-first-order model:

$$q_t = q_e(1 - e^{-K_1 t}) \tag{8}$$

Table 6
(a) Linear and (b) nonlinear Langmuir and Freundlich parameters for the removal of the RhB and OII by the adsorbents studied

Adsorbent	Adsorbate	Langmuir				Freundlich		
		b (mg/g)	K_L (L/mg)	R_L	R^2	K_F (mg/g)	n	R^2
(a) Linear Langmuir and Freundlich parameters								
JB-AC	RhB	250	0.666	0.0006	0.99	150.31	13.51	0.95
	OII	500	0.666	0.0003	0.99	370.68	18.86	0.94
MK-AC	RhB	142.85	0.212	0.0020	0.99	93.32	13.15	0.9
	OII	333.33	0.75	0.0003	0.99	225.94	20.83	0.89
JB-R	RhB	58.82	0.008	0.0720	0.96	1.72	1.94	0.99
	OII	52.63	0.015	0.0320	0.99	2.20	2.03	0.93
(b) Nonlinear Langmuir and Freundlich parameters								
JB-AC	RhB	207.54	6.36		0.92	152.74	13.32	0.86
	OII	498.5	1.3		0.99	370.62	18.73	0.94
MK-AC	RhB	133.09	47.29		0.96	93.38	13.13	0.92
	OII	297.71	4.355		0.90	226.13	21.03	0.88
JB-R	RhB	68.36	0.0035		0.98	1.73	0.513	0.98
	OII	53.57	0.012		0.98	2.20	0.49	0.94

Table 7
Maximum capacities for adsorption of RhB and OII by various adsorbents

Adsorbate	Adsorbent	Maximum capacity (mg/g)	Reference
RhB	*Maranta arundinacea* AC	88.4	[2]
	Rice husk-based AC	478.5	[41]
	Moringa oleifera bark carbon	114.68	[42]
	Aleurites moluccana seeds	117	[43]
	Jujube stone-AC (JB-AC)	207.5	This study
OII	Titania aerogel	420	[44]
	Tomato waste	312.5	[36]
	Clam shell	1,017.13	[45]
	Rice husk ash	59.1	[46]
	Jujube stone-AC (JB-AC)	498.5	This study

$$\log\left(q_e - q_t\right) = \log q_e - \frac{K_1}{2.303}t \tag{9}$$

- Pseudo-second-order model:

$$q_t = \frac{q_e^2 K_2 t}{1 + q_e K_2 t} \tag{10}$$

$$\frac{t}{q_t} = \frac{1}{K_2 q_e^{\,2}} + \frac{1}{q_e}t \tag{11}$$

- Intraparticle diffusion model:

$$q_t = K_{\text{in}} t^{1/2} + C \tag{12}$$

where q_t and q_e are the adsorption capacities at time t and at equilibrium (mg/g), respectively; K_1 is the rate constant of the pseudo-first-order model for adsorption (min^{-1}), the values of K_1 and q_e were obtained from the slope and intercept of plots of q_t vs. t or $\log(q_e - q_t)$ vs. t. K_2 is the rate constant of the pseudo-second-order model for adsorption (g/mg min), the values of K_2 and q_e were calculated from the slope and intercept of plots of q_t vs. t or t/q_t vs. t. C is the intercept of the q_t vs. $t^{1/2}$ plot and K_{in} is the intraparticle diffusion rate constant ($\text{mg/g min}^{1/2}$).

In order to elucidate the adsorption kinetic process of RhB and OII on all three adsorbents, two different concentrations for each adsorbate were tested. Table 8 summarizes the parameters and coefficients of the pseudo-first-order, pseudo-second-order kinetic and intraparticle diffusion models. The results show that the determination coefficients values (R^2) were close or equal to 1 for the pseudo-second-order model for the linear or nonlinear models. Furthermore, the experimental q_e (q_e(exp)) and the calculated q_e (q_e(cal)) values for both dyes used in this study were very close to one another. On the other hand, calculated values from the linearized pseudo-first-order model did not correspond to experimental values, contrary to nonlinear calculated values, which reflect more realistic situations. It can be said that both kinetic models (pseudo-first-order and pseudo-second-order models) can describe the adsorption kinetics of RhB and OII on the adsorbents investigated, and hence the physical and chemical adsorption processes may both be involved in the overall adsorption process [47,49].

3.6. Removal mechanism

The adsorption process may involve three important steps, namely, film diffusion, intraparticle pore diffusion and the actual adsorption step.

Table 8
(a) Linear and (b) nonlinear kinetic parameters for the adsorption of OII and RhB by adsorbents studied

Dye		Adsorbent					
		JB-AC		MK-AC		JB-R	
(a) Linear kinetic parameters							
RhB	Concentration (mg/L)	1,200	1,300	800	900	10	20
	q_e (exp) (mg/g)	149.92	162.13	99.96	112.23	1.167	2.27
	Pseudo-first-order						
	q_e (calc) (mg/g)	82.03	72.49	11.66	14.22	0.14	0.17
	K_1 (min^{-1})	0.052	0.032	0.043	0.023	0.046	0.039
	R^2	0.99	0.98	0.98	0.97	0.97	0.96
	Pseudo-second-order						
	q_e (calc) (mg/g)	153.84	166.49	100.00	111.11	1.11	2.28
	K_2 (g/mg min)	0.00014	0.0007	0.010	0.003	0.838	0.663
	R^2	0.99	0.99	1	1	1	1
	Intraparticle diffusion						
	K_{in} (mg/g min$^{1/2}$)	1.765	2.922	0.395	1.070	0.022	0.026
	C (mg/g)	132.06	129.90	95.91	100.46	1.001	2.027
	R^2	0.92	0.99	0.97	0.99	0.93	0.97
OII	Concentration (mg/L)	2,800	3,000	1,800	2,000	100	200
	q_e (exp) (mg/g)	349.87	374.42	244.92	249.73	6.01	11.85
	Pseudo-first-order						
	q_e (calc) (mg/g)	15.20	41.59	2.56	12.56	0.17	0.06
	K_1 (min^{-1})	0.041	0.036	0.029	0.027	0.12	0.92
	R^2	0.90	0.91	0.93	0.80	0.94	0.93
	Pseudo-second-order						
	q_e (calc) (mg/g)	350.87	378.78	225.22	250.00	6.02	11.85
	K_2 (g/mg min)	0.006	0.002	0.019	0.006	1.531	0.172
	R^2	1	1	1	1	1	1
	Intraparticle diffusion						
	K_{in} (mg/g min$^{1/2}$)	0.238	1.015	0.099	0.563	0.021	0.170
	C (mg/g)	347.3	363.73	223.87	243.58	5.891	10.817
	R^2	0.99	0.90	0.99	0.98	0.90	0.88
(b) Non linear kinetic parameters							
RhB	Concentration (mg/L)	1,200	1,300	800	900	10	20
	q_e (exp) (mg/g)	149.92	162.13	99.96	112.23	1.167	2.27
	Pseudo-first-order						
	q_e (calc) (mg/g)	148.49	158.39	99.03	109.93	1.093	2.22
	K_1 (min^{-1})	0.0852	0.072	0.0287	0.15045	0.15045	0.626
	R^2	0.99	0.93	0.99	0.97	0.76	0.41
	Pseudo-second-order						
	q_e (calc) (mg/g)	157.95	171.13	100.49	113.18	1.131	2.18
	K_2 (g/mg min)	0.00106	0.0007	0.01016	0.00406	0.406	0.208
	R^2	0.99	0.98	0.99	0.99	0.99	0.41
OII	Concentration (mg/L)	2,800	3,000	1,800	2,000	100	200
	q_e (exp) (mg/g)	349.87	374.42	244.92	249.73	6.01	11.85
	Pseudo-first-order						
	q_e (calc) (mg/g)	349.32	371.68	224.7	248.13	5.99	11.65
	K_1 (min^{-1})	0.18137	0.137	0.24275	0.1988	0.906	0.592
	R^2	0.99	0.91	0.99	0.83	0.60	0.77
	Pseudo-second-order						
	q_e (calc) (mg/g)	354.28	382.5	225.99	250	6.02	11.88
	K_2 (g/mg min)	0.0025	0.00108	0.001024	0.1	1.996	0.2285
	R^2	0.99	0.99	0.99	0.99	0.90	0.96

The diffusion mechanism of the adsorption cannot be identified by the pseudo-first-order and pseudo-second-order kinetic models, and the kinetic results can be analyzed by applying the intraparticle diffusion model [50]. Applying this model, the plots q_t vs. $t^{1/2}$ by Weber and Morris [48] for two solute concentrations were used to calculate K_{in} from the slope and the C parameter are also reported in Table 8. In Fig. 11, the linear plots (q_t vs. $t^{1/2}$) did not pass through the origin, showing that the intraparticle diffusion was not the only rate controlling step [51,52]. The surface chemistry is as important as the specific surface area in the dye removal process. The presence of electron rich groups (carboxyls and carbonyls) on the surface of the activated carbon may be responsible for electrostatic interactions with electronegative groups of the RB molecule, but hydrogen bonding along with weak van der Waals forces may also be involved. As for OII, interactions between carboxyls and the positively charged groups (OH_2^+ and $-NN^+$) present on the dye molecule can account for the strong adsorption process observed. Since both physical and chemical kinetic models can be applied, it can be noted that the removal mechanism is a complex phenomenon as observed in different works [30,36].

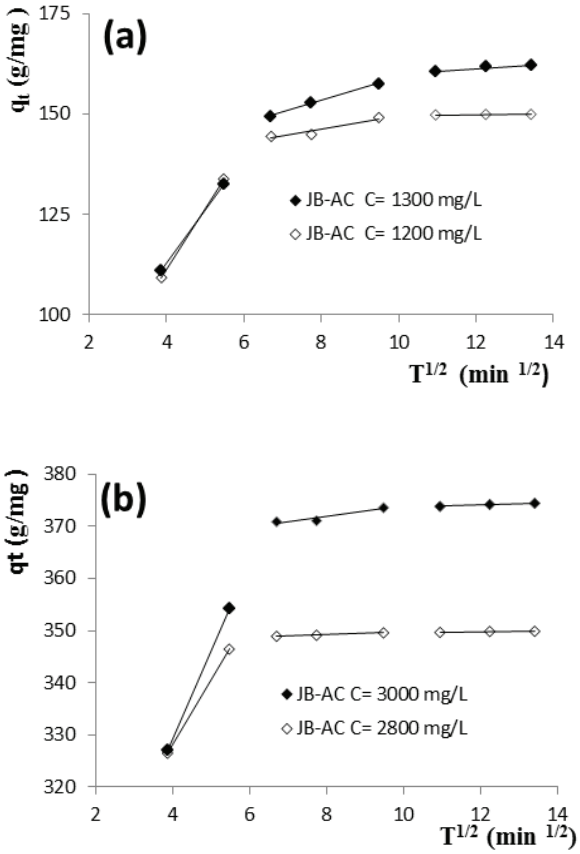

Fig. 11. Plots intraparticle diffusion model of (a) RhB and (b) OII adsorption.

3.7. Thermodynamic parameters

Thermodynamic parameters such as the standard enthalpy change ($\Delta H°$), the standard entropy change ($\Delta S°$) and the Gibbs' free energy change ($\Delta G°$) were determined to estimate the effect of temperature on the adsorption of the RhB and OII. The thermodynamic parameters were calculated from Eqs. (13)–(15) [53]:

$$K_d = \frac{C_s}{C_{eq}} \tag{13}$$

$$\Delta G° = -RT \ln K_d \tag{14}$$

$$\ln K_d = \frac{\Delta S°}{R} - \frac{\Delta H°}{RT} \tag{15}$$

where R (8.314 J/mol K) denotes the universal gas constant, T (K) is the absolute temperature, K_d the distribution coefficient, C_s is the amount of dye (mg) adsorbed on adsorbent per liter of solution at equilibrium and C_{eq} is the equilibrium dye concentration (mg/L). $\Delta H°$ (kJ/mol) and $\Delta S°$ (kJ/mol K) were obtained from the slope and intercept of the van't Hoff plot of $\ln K_d$ vs. $1/T$ (figures not shown).

Table 9 displays the thermodynamic parameters at three various temperatures (298, 303 and 313 K). The values of $\Delta G°$ were negative, demonstrating spontaneous and thermodynamically favorable adsorption. The adsorption process is viewed as physiosorption, when $\Delta H°$ is less than 20 kJ/mol, as chemisorption when $\Delta H°$ is in the range of 80–200 kJ/mol according to previous reports [41,54]. The results show that $\Delta H°$ of RhB and OII onto JB-AC was between 83.96 and 101.77 kJ/mol and adsorption process was endothermic. The values of $\Delta H°$ between 20 and 80 kJ/mol suggest that the adsorption of RhB and OII on MK-AC was rather physiosorption. The positive values of $\Delta S°$ suggest increased randomness at the solid–liquid interface as adsorption occurs.

Table 9
Thermodynamic parameters for the adsorption of OII and RhB by adsorbents studied

Adsorbate	Adsorbent	$-\Delta G°$ (kJ/mol)			$\Delta H°$ (kJ/mol)	$\Delta S°$ (kJ/mol K)
		298 (K)	303 (K)	313 (K)		
RhB	JB-AC	14.449	16.102	20.241	101.769	0.390
	MK-AC	10.792	12.626	15.381	79.119	0.302
	JB-R	1.394	1.547	1.837	7.4	0.03
OII	JB-AC	12.838	14.826	17.781	83.967	0.325
	MK-AC	8.184	8.991	11.144	51.36	0.200

4. Conclusion

This study has dealt with the removal of RhB and OII dyes from their aqueous solutions by activated carbon prepared from jujube stones. The activated carbon prepared under the following conditions: The jujube stones char prepared at 500°C during 60 min, impregnation ratio 2:1 (KOH:char) and 700°C carbonization temperature for a 3 h activation time exhibited high porosity with a surface area, iodine number and methylene blue index of 1,400 m^2/g, 1,358 mg/g and 299 mg/g, respectively. Equilibrium adsorption data were well defined by the Langmuir isotherm model for the adsorbents investigated. The maximum adsorption capacities of RhB and OII were 207.5 and 498.5 mg/g onto the prepared jujube stone activated carbon while corresponding values of 133.09 and 297.7 mg/g were obtained for the commercial Merck activated carbon. Moreover, adsorption kinetics of both dyes was successfully described by both the pseudo-first-order and pseudo-second-order rate models for the adsorbents investigated.

The calculated thermodynamic parameters ($\Delta G°$, $\Delta H°$ and $\Delta S°$) showed that adsorption of RhB and OII on both activated carbons was spontaneous and endothermic.

The highly developed porosity as well as the high surface area obtained for the activated carbon prepared from jujube stones resulted in high dye removal capacity, which makes it a promising novel adsorbent that can be utilized successfully for treating dye-laden industrial effluents.

References

[1] A. Demirbas, Agricultural based activated carbons for the removal of dyes from aqueous solutions: a review, J. Hazard. Mater., 167 (2009) 1–9.

[2] M. Ilayaraja, N.P. Krishnan, R. Sayee Kannan, Adsorption of Rhodamine-B and Congo red dye from aqueous solution using activated carbon: kinetics, isotherms, and thermodynamics, IOSR J. Environ. Sci. Toxicol. Food Technol., 5 (2013) 79–89.

[3] M.P. Shah, K.A. Patel, S.S. Nair, A.M. Darji, S. Maharaul, Microbial degradation of Azo dye by *Pseudomonas* spp. MPS-2 by an application of sequential microaerophilic & aerobic process, Am. J. Microbiol. Res., 1 (2013) 105–112.

[4] S.S. Moghaddam, M.R.A. Moghaddam, M. Arami, Coagulation/flocculation process for dye removal using sludge from water treatment plant: optimization through response surface methodology, J. Hazard. Mater., 175 (2010) 651–657.

[5] B. Rodrıguez-Cabo, I. Rodrıguez-Palmeiro, R. Rodil, E. Rodil, A. Arce, A. Soto, Synthesis of AgCl nanoparticles in ionic liquid and their application in photodegradation of Orange II, J. Mater. Sci., 50 (2015) 3576–3585.

[6] M. Abbasi, N.R. Asl, Sonochemical degradation of Basic Blue 41 dye assisted by nanoTiO_2 and H_2O_2, J. Hazard. Mater., 153 (2008) 942–947.

[7] L. Fan, Y. Zhou, W. Yang, G. Chen, F. Yang, Electrochemical degradation of aqueous solution of Amaranth azo dye on ACF under potentiostatic model, Dyes Pigm., 76 (2008) 440–446.

[8] M. Benadjemia, L. Millière, L. Reinert, N. Benderdouche, L. Duclaux, Preparation, characterization and Methylene Blue adsorption of phosphoric acid activated carbons from globe artichoke leaves, Fuel Process. Technol., 92 (2011) 1203–1212.

[9] M. Ghaedi, B. Sadeghian, A.A. Pebdani, R. Sahraei, A. Daneshfar, C. Duran, Kinetics, thermodynamics and equilibrium evaluation of direct yellow 12 removal by adsorption onto silver nanoparticles loaded activated carbon, Chem. Eng. J., 187 (2012) 133–141.

[10] C. Djilani, R. Zaghdoudi, F. Djazi, B. Bouchekima, A. Lallam, A. Modarressi, M. Rogalski, Adsorption of dyes on activated carbon prepared from apricot stones and commercial activated carbon, J. Taiwan Inst. Chem. Eng., 53 (2015) 112–121.

[11] M.A. Ahmad, N.A.A. Puad, O.S. Bello, Kinetic, equilibrium and thermodynamic studies of synthetic dye removal using pomegranate peel activated carbon prepared by microwave-induced KOH activation, Water Resour. Ind., 6 (2014) 18–35.

[12] J. Gao, Y. Qin, T. Zhou, D. Cao, P. Xu, D. Hochstetter, Y. Wang, Adsorption of methylene blue onto activated carbon produced from tea (*Camellia sinensis* L.) seed shells: kinetics, equilibrium, and thermodynamics studies, J. Biomed. Biotechnol., 14 (2013) 650–658.

[13] P.K. Malik, Use of activated carbons prepared from sawdust and rice-husk for adsorption of acid dyes: a case study of Acid Yellow 36, Dyes Pigm., 56 (2003) 239–249.

[14] M.M. Hamed, M.M.S. Ali, M. Holiel, Preparation of activated carbon from doum stone and its application on adsorption of ^{60}Co and $^{152+154}Eu$: equilibrium, kinetic and thermodynamic studies, J. Environ. Radioact., 164 (2016) 113–124.

[15] I.A.W. Tan, A.L. Ahmad, B.H. Hameed, Adsorption of basic dye using activated carbon prepared from oil palm shell: batch and fixed bed studies, Desalination, 225 (2008) 13–28.

[16] G.O. El-Sayed, M.M. Yehia, A.A. Asaad, Assessment of activated carbon prepared from corncob by chemical activation with phosphoric acid, Water Resour. Ind., 7–8 (2014) 66–75.

[17] N. Bouchelkia, L. Mouni, L. Belkhiri, A. Bouzaza, J. Bollinger, K. Madani, F. Dahmoun, Removal of lead(II) from water using activated carbon developed from jujube stones, a low-cost sorbent, Sep. Sci. Technol., 51 (2016) 1645–1653.

[18] H.M. Chiang, T.C. Chen, S.D. Pan, H.L. Chiang, Adsorption characteristics of Orange II and chrysophenine on sludge adsorbent and activated carbon fibers, J. Hazard. Mater., 161 (2009) 1384–1390.

[19] N. Douara, B. Bestani, N. Benderdouche, L. Duclaux, Sawdust-based activated carbon ability in the removal of phenol-based organics from aqueous media, Desal. Wat. Treat., 57 (2016) 5529–5545.

[20] J. Jagiello, J.P. Olivier, A simple two-dimensional NLDFT model of gas adsorption in finite carbon pores. Application to pore structure analysis, J. Phys. Chem. C, 113 (2009) 19382–19385.

[21] J. Jagiello, M. Thommes, Comparison of DFT characterization methods based on N_2, Ar, CO_2, and H_2 adsorption applied to carbons with various pore size distributions, Carbon, 42 (2004) 1227–1232.

[22] S. Attouti, B. Bestani, N. Benderdouche, D. Laurent, Application of *Ulva lactuca* and *Systoceira stricta* algae-based activated carbons to hazardous cationic dyes removal from industrial effluents, Water Res., 47 (2013) 3375–3388.

[23] A. Belayachi, B. Bestani, A. Bendraoua, N. Benderdouche, L. Duclaux, The influence of surface functionalization of activated carbon on dyes and metal ion removal from aqueous media, Desal. Wat. Treat., 57 (2016) 17557–17569.

[24] Y. Shinogi, Y. Kanri, Pyrolysis of plant, animal and human waste: physical and chemical characterization of the pyrolytic products, Bioresour. Technol., 90 (2003) 241–247.

[25] D. Angın, Effect of pyrolysis temperature and heating rate on biochar obtained from pyrolysis of safflower seed press cake, Bioresour. Technol., 128 (2013) 593–597.

[26] P. Chuenklang, S. Thungtong, T. Vitidsant, Effect of activation by alkaline solution on properties of activated carbon from rubber wood, J. Met. Mater. Miner., 12 (2002) 29–38.

[27] W.M.A.W. Daud, W.S.W. Ali, M.Z. Sulaiman, Effect of activation temperature on pore development in activated carbon produced from palm shell, J. Chem. Technol. Biotechnol., 78 (2002) 1–5.

[28] S.M. Yakout, G. Sharaf El-Deen, Characterization of activated carbon prepared by phosphoric acid activation of olive stones, Arabian J. Chem., 9 (2016) S1155–S1162.

[29] L.Y. Meng, S.J. Park, Investigation of narrow pore size distribution on carbon dioxide capture of nanoporous carbons, Bull. Korean Chem. Soc., 33 (2012) 3749–3754.

[30] M. Mohammadi, A.J. Hassani, A.R. Mohamed, G.D. Najafpour, Removal of Rhodamine B from aqueous solution using palm shell-based activated carbon: adsorption and kinetic studies, J. Chem. Eng. Data, 55 (2010) 5777–5785.

[31] C. Xu, N. Hedin, Ultramicroporous CO_2 adsorbents with tunable mesopores based on polyimines synthesized under

off-stoichiometric conditions, Microporous Mesoporous Mater., 222 (2016) 80–86.
[32] D. Graham, Characterization of physical adsorption systems III. The separate effects of pore size and surface acidity upon the adsorbent capacities of activated carbons, J. Phys. Chem., 59 (1955) 896–900.
[33] M.R.R. Kooh, M.K. Dahri, L.B.L. Lim, The removal of Rhodamine B dye from aqueous solution using *Casuarina equisetifolia* needles as adsorbent, Cogent Environ. Sci., 2 (2016) 1–14.
[34] N. Thinakaran, P. Baskaralingam, M. Pulikesi, P. Panneerselvam, S. Sivanesan, Removal of acid violet 17 from aqueous solutions by adsorption onto activated carbon prepared from sunflower seed hull, J. Hazard. Mater., 151 (2008) 316–322.
[35] Z.M. Abou-Gamra, H.A.A. Medien, Kinetic, thermodynamic and equilibrium studies of Rhodamine B adsorption by low cost biosorbent sugar cane bagasse, Eur. Chem. Bull., 2 (2013) 417–422.
[36] F. Güzel, H. Sayğılı, G.A. Sayğılı, F. Koyuncu, Elimination of anionic dye by using nanoporous carbon prepared from an industrial biowaste, J. Mol. Liq., 194 (2014) 130–140.
[37] A.A. Said, A.A.M. Aly, M.M. Abd El-Wahab, S.A. Soliman, A.A. Abd El-Hafez, V. Helmey, M.N. Goda, Potential application of propionic acid modified sugarcane bagasse for removing of basic and acid dyes from industrial wastewater, Resour. Environ., 2 (2012) 93–99.
[38] I. Langmuir, The adsorption of gases on plane surfaces of glass, mica and platinum, J. Am. Chem. Soc., 40 (1918) 1361–1403.
[39] M. Arami, N.Y. Limaee, N.M. Mahmoodia, Evaluation of the adsorption kinetics and equilibrium for the potential removal of acid dyes using a biosorbent, Chem. Eng. J., 139 (2008) 2–10.
[40] H. Freundlich, Of the adsorption of gases. Section II. Kinetics and energetics of gas adsorption. Introductory paper to section II, Trans. Faraday Soc., 28 (1932) 195–201.
[41] L. Ding, B. Zou, W. Gao, Q. Liu, Z. Wang, Y. Guo, X. Wang, Y. Liu, Adsorption of Rhodamine-B from aqueous solution using treated rice husk-based activated carbon, Colloids Surf., A, 446 (2014) 1–7.
[42] S. Ramuthai, V. Nandhakumar, M. Thiruchelvi, S. Arivoli, V. Vijayakumaran, Rhodamine B adsorption-kinetic, mechanistic and thermodynamic studies, J. Chem., 6 (2009) S363–S373.
[43] D.L. Postai, C.A. Demarchi, F. Zanatta, D.C.C. Melo, C.A. Rodrigues, Adsorption of rhodamine B and methylene blue dyes using waste of seeds of *Aleurites Moluccana*, a low cost adsorbent, Alexandria Eng. J., 55 (2016) 1713–1723.
[44] L. Abramian, H. El-Rassy, Adsorption kinetics and thermodynamics of azo-dye Orange II onto highly porous titania aerogel, Chem. Eng. J., 150 (2009) 403–410.
[45] J. Ma, J. Zou, B. Cui, C. Yao, D. Li, Adsorption of Orange II dye from aqueous solutions using phosphoric-acid modified clam shell powder, Desal. Wat. Treat., 51 (2013) 6536–6544.
[46] X.G. Chen, S.S. Lv, Y. Ye, J.P. Cheng, S.H. Yin, Preparation and characterization of rice husk/ferrite composites, Chin. Chem. Lett., 21 (2010) 122–126.
[47] K.V. Kumar, Linear and non-linear regression analysis for the sorption kinetics of methylene blue onto activated carbon, J. Hazard. Mater., 137 (2006) 1538–1544.
[48] W.J. Weber Jr., J.C. Morris, Kinetics of adsorption on carbon from solution, J. Sanit. Eng. Div. ASCE, 89 (1963) 31–59.
[49] B. Koumanova, P. Peeva-Antova, Z. Yaneva, Adsorption of 4-chlorophenol from aqueous solutions on activated carbon – kinetic study, J. Univ. Chem. Technol. Metall., 40 (2005) 213–218.
[50] A.S. Ozcan, B. Erdem, A. Ozcan, Adsorption of Acid Blue 193 from aqueous solutions onto BTMA-bentonite, Colloids Surf., A, 266 (2005) 73–81.
[51] K. Liu, H. Li, Y. Wang, X. Gou, Y. Duan, Adsorption and removal of Rhodamine B from aqueous solution by tannic acid functionalized graphene, Colloids Surf., A, 477 (2015) 35–41.
[52] P. Panneerselvam, N. Morad, K.A. Tan, R. Mathiyarasi, Removal of Rhodamine B dye using activated carbon prepared from Palm Kernel Shell and Coated with iron oxide nanoparticles, Sep. Sci. Technol., 47 (2012) 742–752.
[53] A. Ouldmoumna, L. Reinert, N. Benderdouche, B. Bestani, L. Duclaux, Characterization and application of three novel biosorbents *Eucalyptus globulus*, *Cynara cardunculus*, and *Prunus cerasefera* to dye removal, Desal. Wat. Treat., 51 (2013) 3527–3538.
[54] Q. Li, Q.-Y. Yue, Y. Su, B.-Y. Gao, H.-J. Sun, Equilibrium, thermodynamics and process design to minimize adsorbent amount for the adsorption of acid dyes onto cationic polymer-loaded bentonite, Chem. Eng. J., 158 (2010) 489–497.